Enhanced Control of Transient Raman Scattering Using Buffered Hydrogen in Hollow-Core Photonic Crystal Fibers

P. Hosseini,[1] D. Novoa,[1] A. Abdolvand,[1] and P. St. J. Russell[1,2]
[1]Max Planck Institute for the Science of Light, Staudtstraße 2, 91058 Erlangen, Germany
[2]Department of Physics, University of Erlangen-Nuremberg, 91058 Erlangen, Germany
(Received 23 June 2017; published 21 December 2017)

Many reports on stimulated Raman scattering in mixtures of Raman-active and noble gases indicate that the addition of a dispersive buffer gas increases the phase mismatch to higher-order Stokes and anti-Stokes sidebands, resulting in a preferential conversion to the first few Stokes lines, accompanied by a significant reduction in the Raman gain due to collisions with gas molecules. Here we report that, provided the dispersion can be precisely controlled, the effective Raman gain in a gas-filled hollow-core photonic crystal fiber can actually be significantly enhanced when a buffer gas is added. This counterintuitive behavior occurs when the nonlinear coupling between the interacting fields is strong and can result in a performance similar to that of a pure Raman-active gas, but at a much lower total gas pressure, allowing competing effects such as Raman backscattering to be suppressed. We report high modal purity in all the emitted sidebands, along with anti-Stokes conversion efficiencies as high as 5% in the visible and 2% in the ultraviolet. This new class of gas-based waveguide device, which allows the nonlinear optical response to be beneficially pressure-tuned by the addition of buffer gases, may find important applications in laser science and spectroscopy.

DOI: 10.1103/PhysRevLett.119.253903

Mixtures of atomic and molecular gases have been useful for improving the efficiency of high-harmonic generation [1], controlling the spatial distribution of multiple filaments [2], and increasing the output power of copper-vapor lasers [3]. It has also been shown that the addition of a noble buffer gas to a Raman-active gas increases the phase mismatch for the generation of higher-order sidebands in stimulated Raman scattering (SRS), restricting the conversion to the first few Stokes lines [4,5]. Most of these studies, carried out in free-space arrangements, were performed in the steady-state regime of SRS, when the Raman gain falls as a result of collisional broadening at higher partial buffer gas pressures. This gain reduction can, however, be drastically mitigated in a gas-filled hollow-core photonic crystal fiber (HC PCF), which offers long collinear interaction lengths at a high pump intensity, permitting operation in the so-called transient SRS regime, when the duration of the pump pulses is comparable to the lifetime of the molecular oscillations T_2 [6]. This can lead to the generation of spectral clusters in HC PCFs filled with gas mixtures [7].

In this Letter, we report that the nonlinear optical response of gas mixtures can be dramatically modified when they are confined in broadband-guiding HC PCFs. As a confirmation of the value of this new approach to gas-based nonlinear fiber optics, we show that the effective Raman gain of a molecular-atomic mixture can actually be significantly higher than in a pure gas, and at much lower total pressures. This counterintuitive phenomenon, which uniquely allows the efficient generation of Raman sidebands from the ultraviolet to the near infrared in an LP_{01}-like guided mode, is the result of the interplay of the normal gas dispersion and the spectrally smooth and anomalous hollow waveguide dispersion. This strongly affects the net Raman gain. The effect is strongest in the vicinity of the zero dispersion point, when coupling between the pump, Stokes, and anti-Stokes fields is strong [8,9]—conditions that are very difficult if not impossible to arrange in a collinear free-space geometry. Moreover, a precise adjustment of the partial pressure of the buffer gas reduces the influence of parasitic effects such as Raman backscattering and amplification of higher-order modes.

We report a series of experiments on vibrational SRS (frequency shift 125 THz) in which a precisely prepared mixture of H_2 and Xe is introduced into a short length of kagome-style HC PCF. Pumping the fiber at 532 nm results in conversion efficiencies of 5% to the 435 nm anti-Stokes and 2% to the 368 nm second anti-Stokes bands. Remarkably, all the sidebands are emitted in the fundamental LP_{01}-like core mode, in sharp contrast to previous studies [10,11].

In the limit of no pump depletion, the steady-state exponential gain factor for Stokes light in the LP_{01}-like mode, pumped in the LP_{01}-like mode, is $G_{01}^{SS} = \rho_{01} S_{01} g_P I_P L$, where g_P is the vibrational Raman gain in bulk hydrogen ($g_P \propto T_2$) [8], S_{ij} is the nonlinear spatial overlap integral between the LP_{01}-like pump mode and the LP_{ij}-like Stokes mode ($S_{01} = 1$ in our system, because both pump and Stokes beams are predominantly guided in the LP_{01} mode), $\rho_{01} \leq 1$ is the gain reduction factor [9], I_P

is the pump intensity, and L is the fiber length [8]. In the steady state, g_P saturates at pressures above 10 bar, i.e., above the Dicke narrowing pressure [12,13]. This is, however, no longer the case if the system operates in the transient regime, which holds when the following conditions are satisfied: $g_P I_P L \gg \hat{\tau}_P$ and $g_P I_P L \gg 1/\hat{\tau}_P$, where $\hat{\tau}_P = \tau_P/T_2$, τ_P being the duration of a square pump pulse. Provided these two conditions are satisfied (always the case in our experiments), the power amplification factor of the Stokes signal in bulk gas can be written [14]

$$\left|\frac{E_S(L)}{E_S(0)}\right|^2 \simeq \frac{1}{\pi}\frac{\exp(\sqrt{8 g_P I_P L \hat{\tau}_P})}{\sqrt{8 g_P I_P L \hat{\tau}_P}} e^{-2\hat{\tau}_P}. \quad (1)$$

The transient exponential gain factor in the fiber can then be written

$$G_{01}^{\mathrm{TR}} = \sqrt{8 g_P \rho_{01} S_{01} I_P L \hat{\tau}_P} - 2\hat{\tau}_P. \quad (2)$$

Although increasing the buffer gas pressure will increase the second term, for large enough values of $I_P L$ (easily attainable in HC PCF) the first term will dominate [7]. This means that the system can operate in the transient regime even with nanosecond pulse durations [6].

While negligibly affecting the material gain, the buffer gas predominantly modifies the fiber dispersion and thus the gain reduction factor, through $\rho_{01} \propto \vartheta_{01}/g_P I_P$, where $\vartheta_{01} = (\beta_S^{01} + \beta_{\mathrm{AS}}^{01}) - 2\beta_P^{01}$ is the dephasing rate and β_J^{01} is the propagation constant of the Jth sideband traveling in the LP_{01}-like mode [8]. To illustrate this, we explore in Fig. 1 the dependence of G_{01}^{TR} on the pump intensity and partial pressure, in a kagome PCF with 11 μm core radius and 90 nm core-wall thickness, pumped at 532 nm with 1 ns pulses. For these parameters, coherent Raman gain suppression ($\rho_{01} = 0$, i.e., $\vartheta_{01} = 0$) occurs at a partial pressure of hydrogen $p_{\mathrm{H_2}} \sim 18$ bar [9]. Figure 1(a) shows, for fixed $I_P = 15\ \mathrm{W}/\mu\mathrm{m}^2$, the pressure at which $\rho_{01} = 0$ can be tuned simply by increasing the partial pressure of the buffer gas p_{Xe} at any value of $p_{\mathrm{H_2}} < 18$ bar. Similarly, when $p_{\mathrm{H_2}}$ is fixed at 15 bar [Fig. 1(b)], the gain is strongly enhanced with increasing pump intensity, especially in the vicinity of $p_{\mathrm{Xe}} \sim 4$ bar.

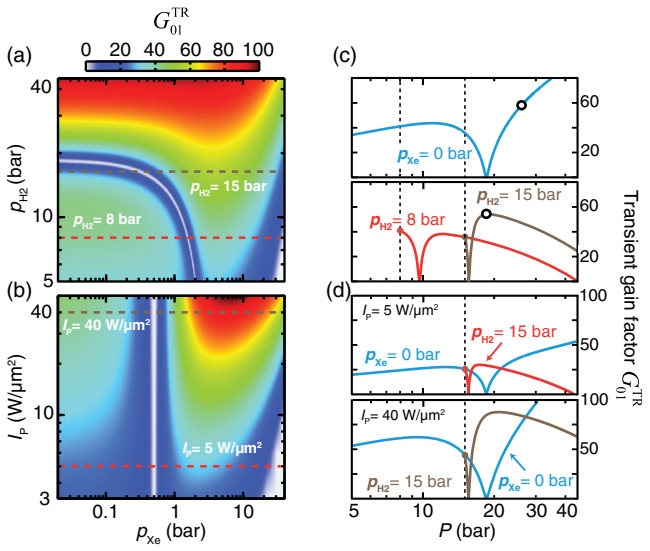

FIG. 1. Transient exponential gain factor G_{01}^{TR} plotted against (a) $p_{\mathrm{H_2}}$ and p_{Xe} for $I_p = 15\ \mathrm{W}/\mu\mathrm{m}^2$ and (b) I_P and p_{Xe} for $p_{\mathrm{H_2}} = 15$ bar. (c) and (d) are cuts through at the positions of the horizontal dashed lines in (a) and (b), respectively. The blue curves in (c) and (d) show the behavior when $p_{\mathrm{Xe}} = 0$.

The lower panel in Fig. 1(c) shows horizontal slices through Fig. 1(a) at $p_{\mathrm{H_2}} = 8$ and 15 bar (note that they are plotted against the total pressure $P = p_{\mathrm{H_2}} + p_{\mathrm{Xe}}$). The upper panel shows the behavior when $p_{\mathrm{Xe}} = 0$ (pure hydrogen). It is clear that, whereas G_{01}^{TR} in the gas mixture qualitatively follows the same behavior as pure hydrogen, i.e., the gain drops to zero at $\vartheta_{01} = 0$ and recovers as the pressure increases, it exhibits a number of interesting and unique features. For example, the higher dispersion of Xe means that the gas pressure P required for gain recovery, i.e., $\rho_{01} \sim 1$, can be much lower than in the case of pure hydrogen. For instance, $\rho_{01} > 0.9$ is achieved at a pressure of ~38 bar for pure hydrogen [upper panel in Fig. 1(c)] and ~17 bar for the mixture with $p_{\mathrm{H_2}} = 15$ bar [brown curve in the lower panel in Fig. 1(c)]. Note that the slight reduction in gain at higher Xe pressures is due to a reduction in $T_2 \propto \hat{\tau}_P^{-1}$ [Eq. (2)].

Another interesting feature is that G_{01}^{TR} can actually be enhanced by the addition of a buffer gas. For instance, the maximum gain for $p_{\mathrm{H_2}} = 15$ bar, represented by the brown solid curve in Fig. 1(c), reaches a value comparable to that obtained with 25 bar of pure $\mathrm{H_2}$ at $p_{\mathrm{Xe}} \sim 3$ bar (marked with black circles), a somewhat counterintuitive result, since the density of $\mathrm{H_2}$ does not change as p_{Xe} increases. This is because the effective Raman gain [Eq. (2)] must be considered, not the material gain [8]. The addition of buffer gas frustrates coherent gain suppression by increasing the dephasing rate, making it possible to recover a value close to that of the material gain ($\rho_{01} \sim 1$). This increase in the gain is even more pronounced at high pump intensities [see Fig. 1(b)]—an important feature in the design of fiber-based Raman shifters and Raman comb generators [22,23]. Figure 1(d) also shows horizontal slices of Fig. 1(b) for two

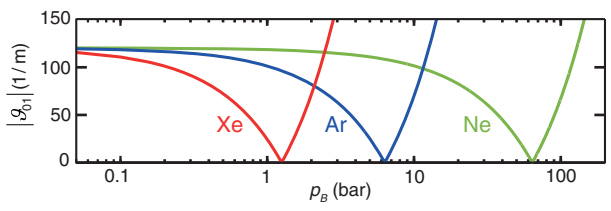

FIG. 2. Dephasing rate for different $\mathrm{H_2}$–noble-gas mixtures at $p_{\mathrm{H_2}} = 10$ bar and increasing p_B.

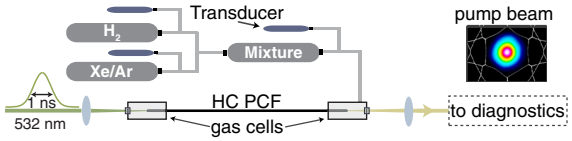

FIG. 3. Schematic diagram of the experiment. The pressure scan was performed in steps of ~100 mbar of buffer gas. The pump beam is mainly launched in the fundamental core mode (near-field image shown in the inset).

different pump intensities of 5 and 40 $W/\mu m^2$ in the upper and lower panel, respectively. These results show that the addition of a noble gas allows the control of the effective in-fiber Raman gain and thus the overall performance of the system.

In Fig. 2, the dephasing rate is plotted versus the buffer gas pressure p_B for the same system as modeled in Fig. 1, when Xe, Ar, or Ne are added ($p_{H_2} = 10$ bar). The differing buffer gas dispersions [24] permit the adjustment of the gain suppression pressure over a wide range—an important feature in the generation of single-mode anti-Stokes sidebands.

To verify these predictions, we built the setup in Fig. 3. A 37-cm length of the kagome PCF mentioned above was pumped with few- microjoule, 1 ns, pulses at 532 nm, generated by a microchip laser. Note that similar results are expected if the kagome PCF is replaced by any other type of antiresonant-reflecting hollow-core PCF. The extremely thin core walls enabled operation in the ultraviolet, since the first anticrossing between the LP_{01}-like core mode and resonances in the core wall lies at 210 nm [25].

To allow precise control of the partial pressures of the mixing gases, we filled each gas species into a separate gas bottle at the required pressure. These gases were then mixed in a separate bottle before being pumped into the fiber. This procedure was essential to ensure homogeneity of the gas mixture—if injected into the fiber separately, the large difference in diffusion rates would cause nonuniform gas concentrations. In addition, we monitored the power of the pump, Stokes, and anti-Stokes bands over time so as to ensure that the system had reached equilibrium before doing any final measurement. Two different sets of experiments were conducted, all of them at a pump pulse energy of 3.6 μJ. First, the fiber was filled with pure H_2 and the pressure varied from 5 to 35 bar [Fig. 4(a)]. Second, p_{H_2} was fixed at 12 [Fig. 4(b)] and 13.5 bar [Fig. 4(c)], and p_{Xe} was swept. The energy in each sideband and the near-field mode profiles were recorded while scanning the pressure. The measured energies of the first Stokes (at 683 nm) and anti-Stokes (at 435 nm) bands are represented by the data points in Fig. 4. The results of numerical simulations (solid curves in Fig. 4) using a multimode-extended set of Maxwell-Bloch equations [14] show very good agreement. As reported in Ref. [8], the Stokes band tends to be emitted in an LP_{11}-like mode when parametric gain suppression is strong for the LP_{01}-like mode.

These results confirm that the behavior of the sidebands qualitatively follows that of the pure gas [Fig. 4(a)], but at a lower total pressure. In particular, the second peak of anti-Stokes, which occurs at 22 bar for pure H_2, appears at 13.6 bar for a H_2/Xe mixture. It is also interesting that using a gas mixture reduces the strength of Stokes emission in the LP_{11}-like mode, at the pressure where conversion to the anti-Stokes band is maximum (see the near-field images in Fig. 4). The presence of the buffer gas causes a slight reduction in the material gain while inhibiting the gain suppression, as explained above. As a result, both Stokes and anti-Stokes bands are emitted in a pure LP_{01}-like mode at the point where the anti-Stokes signal is strongest, a situation that does not occur when there is no buffer gas. Remarkably, the conversion efficiency to the LP_{01} anti-Stokes band, expressed as the ratio between the output energy in the sideband to the input pump energy, reaches 5%, a value which is, to our best knowledge, the highest yet reported in a single-mode fiber-based vibrational H_2 Raman convertor [10]. At $p_{H_2} = 13.5$ bar, the Raman gain is even higher, resulting in ~40% conversion to the Stokes band, comparable to the values obtained with the pure gas at much higher pressures (~25 bar, although for pure H_2 the maximum Stokes emission occurs in a mixture of fiber

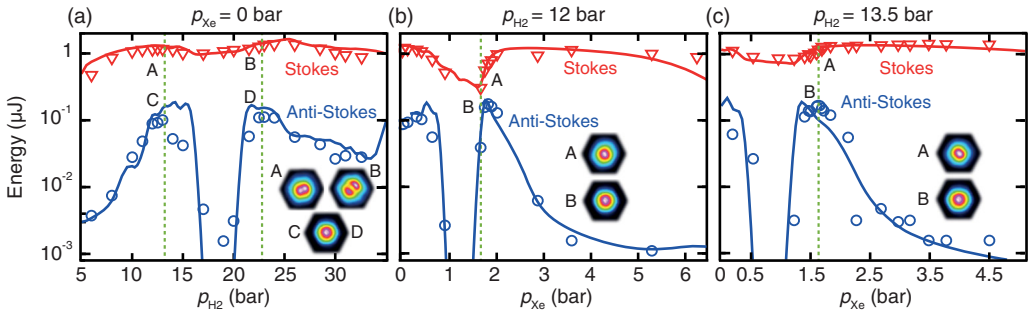

FIG. 4. Experimental (symbols) and simulated (solid lines) energy in the first Stokes and anti-Stokes bands for a pump energy of 3.6 μJ, plotted (a) against p_{H_2} for pure H_2, (b) against p_{Xe} for $p_{H_2} = 12$ bar, and (c) against p_{Xe} for $p_{H_2} = 13.5$ bar. Also shown are near-field optical micrographs of the Stokes and anti-Stokes signals at pressures where the anti-Stokes emission is strongest (shown by the dashed green lines).

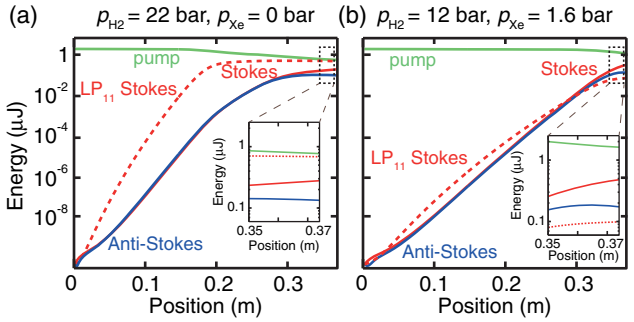

FIG. 5. Simulated evolution of the sideband energies with position at the maximum of anti-Stokes emission and 3.6 μJ pump energy for (a) $p_{H_2} = 22$ bar and $p_{Xe} = 0$ and (b) $p_{H_2} = 12$ bar and $p_{Xe} = 1.6$ bar. The parameters are otherwise identical to those in Fig. 4. The dashed red curve shows the LP_{11}-like Stokes signal, and the insets plot the evolution over the last 2 cm of fiber.

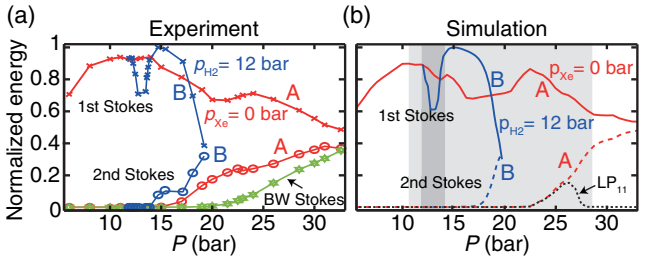

FIG. 6. (a) Measured energies in the first (crosses) and second (circles) Stokes signals for 5.4 μJ pump energy. The red data points (marked A) are for pure hydrogen and the blue (marked B) for a mixture with $p_{H_2} = 12$ bar. The green data points show the backward Stokes energy, measured for $p_{Xe} = 0$. (b) Numerical simulations excluding backward SRS. The dashed brown line shows the second Stokes energy in the LP_{11} mode for $p_{Xe} = 0$.

modes), limited only by the short fiber length [Fig. 4(c)]. The excellent agreement between the simulation and experiment makes it possible to study numerically inaccessible aspects of the system. As an example, Fig. 5 shows the evolution of the three signals along the fiber for 3.6 μJ pump energy. In Fig. 5(a), $p_{H_2} = 22$ bar, and in Fig. 5(b), $p_{H_2} = 12$ bar and $p_{Xe} = 1.6$ bar. At these pressures, $\vartheta_{01} \neq 0$, and the second peak of the anti-Stokes occurs. Both sidebands grow with a similar, moderate value of gain until the pump becomes substantially depleted and amplification ceases [26,27]. In the vicinity of the gain-suppression pressure, however, a strong Stokes signal appears in the LP_{11}-like mode [red-dashed curve in Fig. 5(a)], causing pump depletion and drastically impairing LP_{01} amplification. As stated above, the gain for intermodal SRS is reduced in the gas mixture, favoring Stokes generation in the LP_{01} mode [see Fig. 5(b)].

At higher pump energies (5.4 μJ in Fig. 6), the influence of the buffer gas is even more pronounced, the maximum Stokes conversion clearly exceeding that obtained with the pure gas, while the pressure range over which the LP_{11} contribution to the Stokes band exceeds 10% shrinks significantly. This is illustrated in Fig. 6(b) for a H_2-Xe mixture (dark shaded region) and pure H_2 (light shaded region). The red curves are for $p_{Xe} = 0$, and the blue curves are for $p_{H_2} = 12$ bar and varying p_{Xe}. The numerical simulations in Fig. 6(b) exclude backward SRS, which explains the disparity with the experiment results at high H_2 pressures.

The improvement in the Stokes conversion efficiency and LP_{01} mode purity is evident. We also observe that the second-order Stokes band (at 953 nm) is emitted in the LP_{01} mode, with a strength comparable to that obtained in the pure gas though at half the total pressure. Interestingly, for $p_{Xe} = 0$ the second Stokes signal is initially emitted in the LP_{11} mode, gradually evolving to the LP_{01} mode, just like the first Stokes signal [Fig. 6(b)]. The same behavior is observed for the second anti-Stokes (at 368 nm), where the LP_{01} conversion efficiency reaches ~2% [14], further demonstrating the excellent performance of our system for frequency conversion to the ultraviolet [28]. These results supersede those reported previously [4,5], where a buffer gas was used merely to dephase conversion to higher-order sidebands so as to concentrate conversion to the first Stokes.

A further interesting aspect of the PCF-based system is the onset of a strong backward Stokes signal for pure hydrogen at pressures $> \sim 20$ bar when the pulse length is comparable with the fiber length [green curve in Fig. 6(a)] [29]. This effect is even stronger close to the gain suppression point, because the backward gain is not suppressed. Once again, by the careful addition of buffer gas, the effective gain can be increased without increasing the material gain, resulting in a significant increase in the threshold for backward SRS and suppression of higher-order mode amplification. Finally, in order to confirm the universality of this approach, we also performed experiments using mixtures of hydrogen and argon, finding excellent agreement with our predictions [14].

In conclusion, the combination of waveguide dispersion with gas mixtures offers a novel means of controlling the nonlinear optical response. In particular, the judicious addition of a buffer gas can dramatically reduce the hydrogen pressure required for a given dynamics, increase the conversion efficiency, and significantly enhance the effective Raman gain, as well as suppress Stokes emission into the LP_{11} mode and in the backward direction. Buffering can also enhance the generation of narrowband deep and vacuum ultraviolet signals [28], resulting in very high conversion efficiencies. The results suggest a new approach to boosting the sensitivity of coherent anti-Stokes Raman spectroscopy [30]. Finally, preliminary studies suggest that single-pass anti-Stokes conversion efficiencies as high as 10% can be achieved if a pressure gradient is introduced along the fiber.

[1] M. Sayrac, A. A. Kolomenskii, J. Strohaber, and H. A. Schuessler, J. Opt. Soc. Am. B **32**, 2400 (2015).
[2] B. Alonso, A. Zaïr, J. San Román, O. Varela, and L. Roso, Opt. Express **18**, 15467 (2010).
[3] M. J. Withford, D. J. W. Brown, R. J. Carman, and J. A. Piper, Opt. Lett. **23**, 706 (1998).
[4] A. Luches, V. Nassisi, and M. R. Perrone, Appl. Phys. B **47**, 101 (1988).
[5] A.D Papayannis, G. N. Tsikrikas, and A. A. Serafetinides, Appl. Phys. B **67**, 563 (1998).
[6] F. Benabid, G. Antonopoulos, J. C. Knight, and P. St. J. Russell, Phys. Rev. Lett. **95**, 213903 (2005).
[7] P. Hosseini, A. Abdolvand, and P. St. J. Russell, Opt. Lett. **41**, 5543 (2016).
[8] P. Hosseini, M. K. Mridha, D. Novoa, A. Abdolvand, and P. St. J. Russell, Phys. Rev. Applied **7**, 034021 (2017).
[9] S. T. Bauerschmidt, D. Novoa, and P. St. J. Russell, Phys. Rev. Lett. **115**, 243901 (2015).
[10] B. M. Trabold, A. Abdolvand, T. G. Euser, and P. St. J. Russell, Opt. Express **21**, 29711 (2013).
[11] S. T. Bauerschmidt, D. Novoa, B. M. Trabold, A. Abdolvand, and P. St. J. Russell, Opt. Express **22**, 20566 (2014).
[12] C. S. Wang, Phys. Rev. **182**, 482 (1969).
[13] J. R. Murray and A. Javan, J. Mol. Spectrosc. **42**, 1 (1972).
[14] See Supplemental Material at http://link.aps.org/supplemental/10.1103/PhysRevLett.119.253903 for details on the analytical solution of the Maxwell-Bloch equations and the coupled wave equations used in the simulations, together with expressions for the gain reduction factor, the Raman linewidth, and the experimental results for a H_2/Ar mixture, which includes Refs. [15–21].
[15] M. A. Finger, N. Y. Joly, T. Weiss, and P. St. J. Russell, Opt. Lett. **39**, 821 (2014).
[16] M. G. Raymer and I. A. Walmsley, Prog. Opt. **28**, 181 (1990).
[17] J. F. Reintjes, *Handbook of Laser Science and Technology, Supplement 2: Optical Materials* (CRC, Boca Raton, FL, 1995).
[18] W. K. Bischel and M. J. Dyer, Phys. Rev. A **33**, 3113 (1986).
[19] J. P. Berger, R. Saint-Loup, H. Berger, J. Bonamy, and D. Robert, Phys. Rev. A **49**, 3396 (1994).
[20] M. G. Raymer and J. Mostowski, Phys. Rev. A **24**, 1980 (1981).
[21] M. G. Raymer, I. A. Walmsley, J. Mostowski, and B. Sobolewska, Phys. Rev. A **32**, 332 (1985).
[22] Y. Chen, Z. Wang, Z. Li, W. Huang, X. Xi, and Q. Lu, Opt. Express **25**, 20944 (2017).
[23] F. Couny, F. Benabid, P. J. Roberts, P. S. Light, and M. G. Raymer, Science **318**, 1118 (2007).
[24] A. Börzsönyi, Z. Heiner, M. P. Kalashnikov, A. P. Kovacs, and K. Osvay, Appl. Opt. **47**, 4856 (2008).
[25] J. L. Archambault, R. J. Black, S. Lacroix, and J. Bures, J. Lightwave Technol. **11**, 416 (1993).
[26] J. J. Ottusch, M. S. Mangir, and D. A. Rockwell, J. Opt. Soc. Am. B **8**, 68 (1991).
[27] Z. W. Barber, C. Renner, R. R. Reibel, S. S. Wagemann, W. R. Babbitt, and P. A. Roos, Opt. Express **18**, 7131 (2010).
[28] M. K. Mridha, D. Novoa, S. Bauerschmidt, A. Abdolvand, and P. St. J. Russell, Opt. Lett. **41**, 2811 (2016).
[29] R. H. Stolen, Fiber Integr. Opt. **3**, 21 (1980).
[30] A. B. Fedotov, S. O. Konorov, V. P. Mitrokhin, E. E. Serebryannikov, and A. M. Zheltikov, Phys. Rev. A **70**, 045802 (2004).